Title: Multivariate analysis and extraction of parameters in resistive RAMs using the Quantum Point Contact model

Authors: J.B. Roldán[1], E. Miranda[6], G. González-Cordero[1], P. García-Fernández[1], R. Romero-Zaliz[3], P. González-Rodelas[4], A. M. Aguilera[5], M.B. González[2], F. Jiménez-Molinos[1]

Address:

[1]Departamento de Electrónica y Tecnología de Computadores. Universidad de Granada. Facultad de Ciencias. Avd. Fuentenueva s/n, 18071 GRANADA, Spain. Email: jroldan@ugr.es

[2]Institut de Microelectrònica de Barcelona, IMB-CNM (CSIC), Campus UAB, 08193 Bellaterra, Spain

[3]Departamento de Ciencias de la Computación e Inteligencia Artificial. Universidad de Granada. Escuela Técnica Superior de Ingenierías Informática y de Telecomunicación, 18071 GRANADA, Spain

[4]Departamento de Matemática Aplicada. Universidad de Granada. ETSICCP (Edif. Politécnico). Avd. Fuentenueva s/n, 18071 GRANADA, Spain.

[5]Departamento de Estadística e Investigación Operativa and IEMath-GR. Universidad de Granada. Facultad de Ciencias. Avd. Fuentenueva s/n, 18071 GRANADA, Spain.

[6]Dept. Enginyeria Electrònica. Universitat Autònoma de Barcelona, Edifici Q. 08193 Bellaterra, Spain

Abstract:

A multivariate analysis of the parameters that characterize the reset process in RRAMs has been performed. The different correlations obtained can help to shed light on the current components that contribute in the Low Resistance State (LRS) of the technology considered. In addition, a screening method for the Quantum Point Contact (QPC) current component is presented. For this purpose the second derivative of the current has been obtained using a novel numerical method which allows determining the QPC model parameters. Once the procedure is completed, a whole RS series of thousands of curves is studied by means of a genetic algorithm. The extracted QPC parameter distributions are characterized in depth to get information about the filamentary pathways associated with LRS in the low voltage conduction regime.

Index Terms—Resistive switching memory, RRAM, Quantum Point Contact Model, Conductive filaments, Parameter extraction.

I.-INTRODUCTION

Resistive Random Access Memory (RRAM) shows outstanding features to be considered a promising alternative technology for non-volatile memory applications [1]. Among the wide set of characteristics reported in the literature, the following can be accounted for: good scalability, low power, fast speed, the possibility of fabrication in the form of 3D memory stacks and compatibility with the BEOL of CMOS processes [1-14].

The viability of RRAMs has been proved at the device level and also in the integrated circuit arena as reported in Refs. [15-17]. The advantages of this technology with respect to Flash devices lie on remarkable improvements in the reading/writing speed, endurance, operation power, etc. Nevertheless, several hurdles have to be overcome to incorporate RRAMs into the industrialization lines, e.g.: the poor control of the switching uniformity and the lack of standardized compact models for circuit simulation. The stochastic nature of the switching features implies variations in the forming, set and reset voltages and in the resistance distributions [2, 11, 13, 18], both in the Low Resistance State (LRS) and in the High Resistance State (HRS). Great research efforts are needed to clarify the mechanisms behind the physics of Resistive Switching (RS) and consequently behind the device variability. In terms of modelling for circuit simulation, there is also a long way to go: the introduction and acceptance by the scientific community of general compact models and clear parameter extraction algorithms, inclusion of these models into commercial circuit simulators, the consolidation of a publication corpus to offer alternatives to include the different physical effects that show up in RRAM operation for the technologies under study nowadays [2, 13, 14]… In

this manuscript we deepen into the latest issue in line with previous papers in the literature [18-21].

In particular, a screening method for detecting if a current component, capable of being described by the QPC model [22, 23], is contributing to the current of a certain RRAM device is presented. Furthermore, once the QPC fingerprints have been detected, a method to extract the model parameters is proposed. To do so, we employed Ni/HfO_2/Si devices. These RRAMs have been fabricated using the ALD technique [24] and were simulated and physically described in Ref. [25, 26]. The devices show a non-linear I-V relationship in LRS. The QPC model [22, 25, 27] was proposed in addition to an ohmic component to describe the charge transport in this operation regime. It was found that it worked well from the modelling viewpoint and helped to explain the device behaviour for different operations regimes [25, 27] and temperatures [26]. In RRAM devices showing non-linear I-V curves at low voltages in the LRS, different mechanisms can be thought to be responsible for this non-linearity; e. g., Schottky barriers, hopping conduction in an irregular contact between the filament tip and the electrode, presence of a nanometric constriction in the CF tip to be described by the QPC model, etc. The simultaneous contribution of several of these mechanisms is likely and consequently difficult to unveil under standard current measurements. That is why a numerical method to detect the presence of a current component (one linked to the QPC model in our case) is of utmost convenience.

Since the QPC model has been employed to describe the conduction both in the LRS and HRS [23], the proposed procedure might be used for both

operation regimes; however, for the devices under study here we will only focus on the I-V curves in the LRS at low voltages. In the HRS, since there are no favoured conduction paths, different current mechanisms can take place depending on the dielectric nature, the electric field range and temperature [28, 29]. Taking into consideration all these issues, we find the application of our method extremely complicated. On the contrary, the LRS has been characterized in depth previously [25, 26] and a QPC component is recognizable; so, for the sake of simplicity, we will concentrate our analysis on this component here.

This new approach not only will allow the model parameters extraction but also will help us to deepen into the tunnelling barrier features behind the QPC current component. As it will be shown, we have obtained the QPC model parameters for all the curves in a long series of RS cycles by means of a genetic algorithm. The results will allow the analysis of device variability from a different perspective and the connection between important parameters such as the reset voltage, and others that can be extracted with this technique such as V_{Th_reset} introduced in Ref. [27]. For this purpose a multivariate statistical analysis has been considered.

The fabricated devices and measurement process are described in Section II, the numerical procedure in Section III and the main results and discussion in Section IV. Finally, the conclusions are given in Section V.

II.-DEVICE DESCRIPTION AND MEASUREMENT

The devices measured were unipolar Ni/HfO_2/Si-based resistive RAMs. The RRAMs were fabricated on (100) n-type CZ silicon wafers with resistivity (0.007-0.013) Ω cm using a field-isolated process. Atomic layer deposition at 225ºC using tetrakis (Dimethylamido)-hafnium (TDMAH) and H_2O as precursors was employed to deposit 20nm-thick HfO_2 layers. The top Ni electrode with a 200nm thickness was deposited by magnetron sputtering [24]. A GPIB-controlled HP-4155B semiconductor parameter analyser was used to measure different long series of RS cycles under ramped voltage stress. The Si substrate was grounded and a negative voltage was applied to the Ni electrode.

III.-NUMERICAL METHOD

The numerical procedure developed here is based on the calculation of the second derivative of the experimental I-V curves. In a previous work [27], we showed that a new parameter can be defined employing the first current derivative (see Fig. 1a). The current derivative shows a maximum and, the corresponding voltage was named threshold reset voltage V_{Th_reset}. It was found that this parameter is correlated with the reset voltage; as highlighted there, V_{Th_reset} can be used to estimate to some extent the reset voltage without the need of getting into the operation region where the self-accelerated processes that lead to the conductive filament rupture take place [27].

We introduce now the analysis of the current second derivative (Fig. 1b). See that two maxima show up in this curve. The corresponding voltages were termed V2dmax1 and V2dmax2. After a massive calculation for a complete series of more than 2800 experimental RS cycles, it was found that 80% of the second derivative curves showed two maxima for the voltage range employed. The rest usually showed only one maximum and in a few cases three maxima were observed. As explained in Ref. [27], two conduction mechanisms in series (ohmic conduction and QPC based) are involved. Their different weights in each RS cycle, in addition to the stochastic mechanisms linked to the CF formation and rupture, can lead to the situations analysed here.

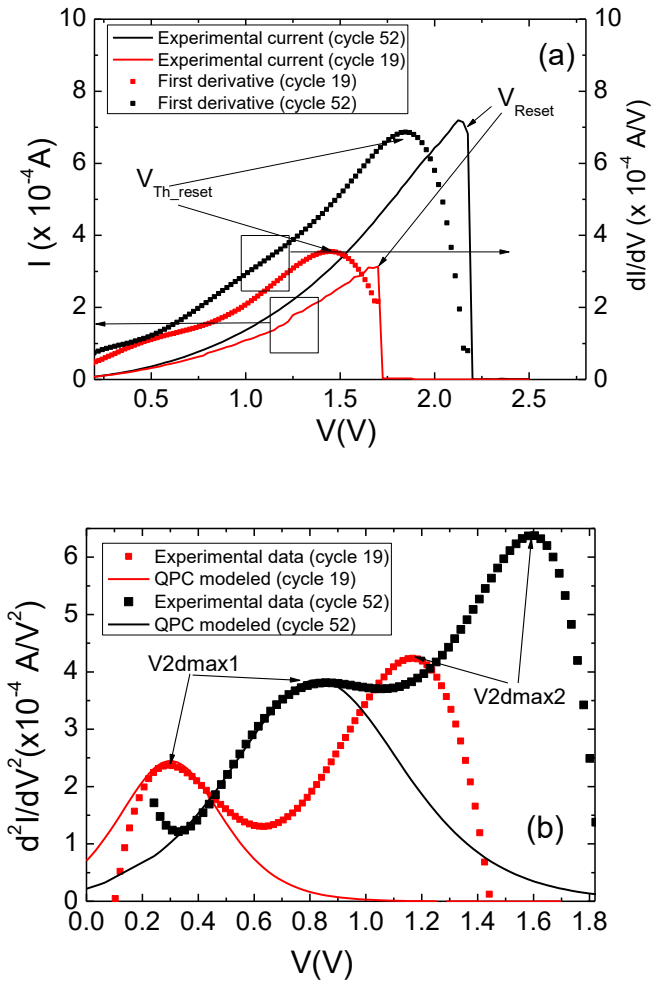

Figure 1: a) Experimental current versus applied voltage in the RRAMs under study and first derivative of the current versus voltage for two reset curves in a long series of RS. Second derivative of the experimental current versus voltage (symbols) for the two reset curves shown in a); the analytically calculated QPC modelled current second derivative (solid lines) is also shown. The parameters under analysis in this manuscript are shown for clarity: V_{Reset}, V_{Th_reset}, V2dmax1, V2dmax2.

In Ref. [27] it was found that at low voltages the resistance component linked to the QPC model, i. e., to a quantum tunnelling conduction regime was the most important component. The current in the QPC model is given by Eq. 1 [22].

$$I = \frac{2eN}{h}\left\{eV_{CTR} + \frac{1}{\alpha}Ln\left[\frac{1+\exp\left\{\alpha\left[\Phi-\beta eV_{CTR}\right]\right\}}{1+\exp\left\{\alpha\left[\Phi+(1-\beta)eV_{CTR}\right]\right\}}\right]\right\} \qquad (1)$$

The Landauer's formalism for 1D quantum conductors and the zero-temperature limit were employed in the deduction of Eq. 1 [22, 30]. The following parameters are used in Eq. 1: Φ, the confinement potential barrier height measured with respect to the equilibrium Fermi level; ∝ describes the curvature of the potential barrier in the longitudinal direction; V_{CTR} is the voltage which is assumed to drop at both ends of the CF constriction (a fraction of β and (1-β) at each extreme [22]); e is the elementary electron charge and N is the number of active channels in the CF (assuming multi-filamentary contribution) [22, 30].

For the devices described in Section II, the ohmic conduction contribution at low voltages is negligible [25, 27]. Therefore, most of the external voltage drops at the ends of the CF constriction described by the QPC model so that $V_{RRAM} \approx V_{CTR}$. Hence, it is reasonable to expect that the device current and its first and second derivatives can be described accurately by the QPC model in this operation regime. We have calculated the second derivative of two of the experimental reset curves in a long RS series, see the curves plotted in symbols in Fig. 1b. The numerical derivative was performed by means of a Weighted Essentially Non Oscillatory (W.E.N.O.) one-dimensional procedure [31, 32]. In this manner, we took advantage of the essentially non-oscillatory nature of the corresponding polynomial interpolation for the calculation. In this approach, a higher accuracy order can be obtained in smooth regions of the data with this procedure [31, 32]. The use of an advanced algorithm based on this technique greatly reduces the numerical oscillations and improves the results of the application of the usual finite differences

techniques, especially when the presence of noise in the data cannot be disregarded (see for example [33]). In relation to this issue, an improvement in the noise treatment was included with respect to the algorithm employed in Ref. [27].

The corresponding analytical second derivative was calculated from Eq. 1. See that the QPC parameters can be tuned to reproduce the low voltage section of the experimental current second derivative around V2dmax1 as shown in Fig. 1b. The presence of the first maximum in the experimental current second derivative and the possibility to fit the curve with the QPC modelled current second derivative suggests that among different transport mechanisms, a QPC-based one is involved. The non-linear I-V relationship at low voltage also supports this assumption [25]. The shape of the current second derivative at low voltages, and most important, the value of V2dmax1 can be employed to obtain information related to the physical features of the transport through the CF constriction modeled by the QPC model. As shown in Fig. 2, were the role played by the different QPC model parameters can be seen in the analytically calculated current second derivative. The position of the curve maximum (V2dmax1) is linked to the parameters β and Φ. The steepness of the curve at the maximum sides is connected to the $\propto$ parameter.

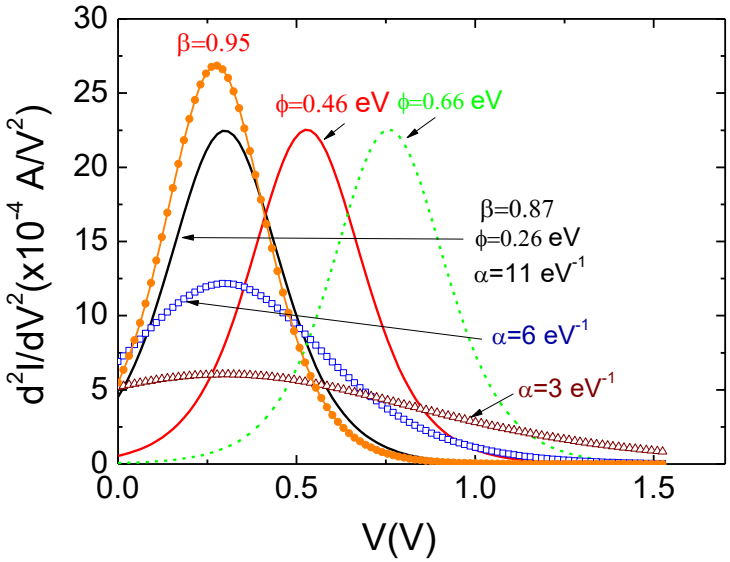

Figure 2: Second derivative of the QPC modeled current described in Eq. 1. The curve shapes for different model parameter values, in the voltage range where they are usually found [22], can be observed. The position of the curve maximum (V2dmax1) is linked to parameters β and Φ. The steepness of the curve at the maximum sides is connected to the ∝ parameter.

It is worth assessing now whether different conduction mechanisms in dielectrics are able or not to reproduce the experimental results. In particular, it is essential to analyse the voltage dependence of these mechanisms and their derivatives. To do so, we have focused the attention on the Poole-Frenkel (PF) and Fowler-Nordheim (FN) components in Fig. 3.

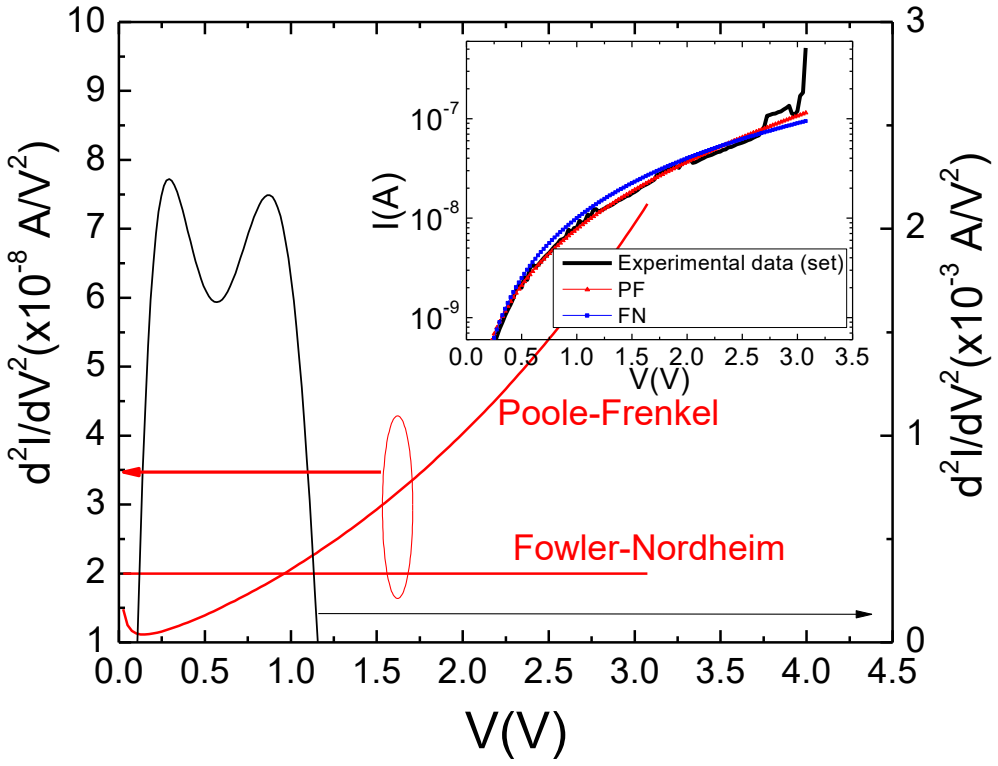

Figure 3: Second derivative of the current versus voltage for two different dielectric conduction mechanisms: Poole-Frenkel and Fowler-Nordheim (red lines). An experimental current curve corresponding to a set cycle has been employed as a reference to obtain the best fit for both current mechanisms, to determine the fitting constants, considering the electric field dependencies of the PF and FN current analytical expressions (see the inset). The experimental current second derivative for the reset curve corresponding to the set curve in the inset has also been plotted in black line for comparison.

We employed a set cycle to obtain the best possible fit for both current components in order to determine their main parameters. Later on, the second derivative was calculated. The current second derivative of the FN presents tree terms, two of them negligible for the constants previously found, the third (the one with the higher value) shows a constant behavior for the voltage range plotted in Fig. 3, see the red curves. The order of magnitude of the current second derivative is much lower than those shown in previous figures and that in black line in Figure 3, since a set cycle has

been employed for the fitting and the current magnitude is much lower than in the reset case.

Apart from PF and FN mechanisms, others could be considered, in particular Schottky emission. In that case, if the electron mean free path is lower than the Schottky barrier width, Simmons modified equation can be employed [29]. Under this assumption an expression analytically similar to the PF current is obtained, except for some differences in the constants. Therefore, a similar second derivative can be expected. In relation to the Space Charge Limited Conduction (SCLC), the ohmic region (low voltages) and the later region (at higher voltages) where Child's square law [29] can be applied will not produce a second derivative comparable to what we showed in Fig. 1b. For ionic conduction, nearest neighbor hopping as well as variable-range hopping no comparable second derivatives are expected since the current analytic dependence on the electric field is linear.

In the devices under study here, at low voltage, as commented below, the ohmic conduction contribution is negligible [25, 27]. This feature can be extended with respect to the considerations connected with the series resistance, although it has been proved that for other devices it could be of importance [23].

The origin of V2dmax2 could be linked to the overlapping of the conduction regimes described by the QPC and ohmic models. In addition, other conduction channels describable by the QPC model might be also important at higher voltages and could contribute to the existence of V2dmax2 in the experimental data.

IV.-RESULTS AND DISCUSSION

A.-Correlations

We have performed the first and second numerical derivatives for more than 2800 reset curves of a continuous RS series. The four parameters shown in Fig. 1 have been obtained and they were represented in Figs. 4 and 5.

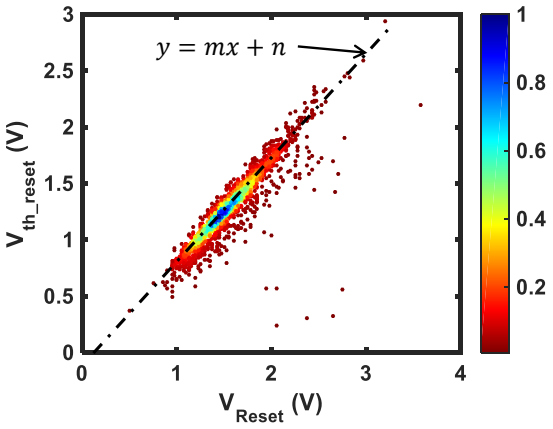

Figure 4: V_{Th_reset} versus V_{Reset} for the devices under study. Data relative to a normalized histogram are shown in a color map. The calculation of the numerical derivatives has been enhanced with respect to Ref. [27]. The dash-dot line shows a linear regression fit with the following parameters m=0.8475, n=-0.0357 V.

A correlation between V_{Th_reset} and V_{Reset} was reported in [27], this correlation is not very clear in connection with V2dmax1, V2dmax2 and V_{Reset} as can be seen in Figure 5. To shed light on this issue, a multivariate analysis of correlation is needed and is presented below. In doing so, the correlation between V_{Th_reset} and V_{Reset} has been revisited within this statistical approach.

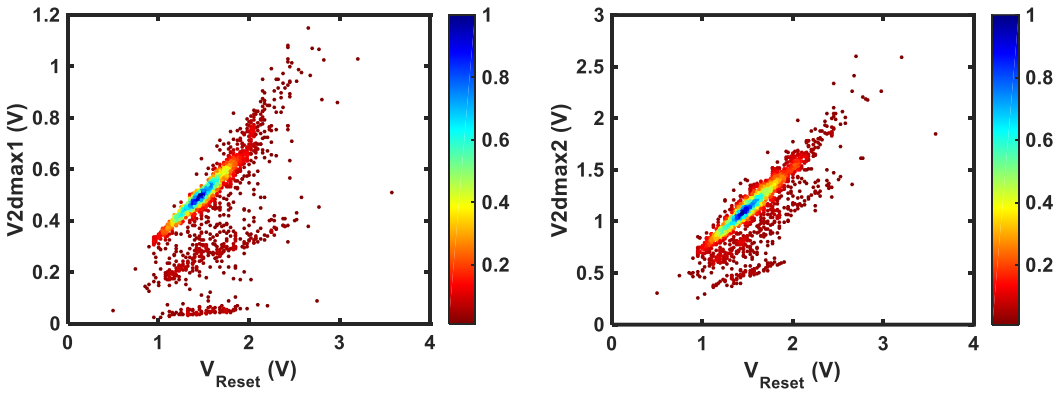

Figure 5: a) V2dmax1 versus V_{Reset} and b) V2dmax2 versus V_{Reset} for the devices under study. Data relative to a normalized histogram are shown in a color map.

It is well known that in the multivariate analysis of statistics [34] we must be aware of the dangers inherent to the interpretation of cross-correlations. In this respect, some of the variables (the parameters under study here) could be confounding variables that, in some sense, explain the relationship between reset voltage and each one of the others parameters (V_{Th_reset}, V2dmax1, V2dmax2). Taking this fact into consideration, computing and interpreting partial correlations for each pair of variables by controlling the others (statistically keeping them constant) is necessary. Summarizing the results obtained for the parameters for each cycle in the long RS series that we are considering, the partial correlations ordered by magnitude in the parameters under analysis are given in Table I.

Parameter	Parameter	Correlation
V2dmax1	V2dmax2	0.826
V_{Reset}	V_{Th_reset}	0.655
V_{Reset}	V2dmax2	0.452
V_{Reset}	V2dmax1	-0.408
V_{Th_reset}	V2dmax2	0.206
V_{Th_reset}	V2dmax1	0.045

Table I. Partial correlations between the different parameters considered in our analysis.

The only partial correlation that keeps the same value than the single correlation is the one between V2dmax1 and V2dmax2 parameters. The other correlations decrease and even change sign when calculating the partial correlations. Therefore, we can conclude that V2dmax1 and V2dmax2 are confounding variables that partly explain the correlation between other variables. V_{Reset} and V_{Th_reset} are also correlated (this was previously observed [27]). In addition, the correlations between V_{Reset} and the maxima of the current second derivative (V2dmax1, V2dmax2) are much smaller but statistically significant. Let us observe that the partial correlation between V_{Reset} and V2dmax1 is negative contrary to the associated single correlation that indicated positive correlation.

Assuming that V2dmax1 is linked to the current QPC modeled component, it is, however, not clear the connection of V2dmax2 with other current components, although we note that it is correlated with V2dmax1. Taking into account that this maximum shows up at higher voltages, a certain link to the ohmic current component is expected; that is why, these two variables, could explain partially the connection between V_{Reset} and V_{Th_reset}. In this manuscript we will focus on V2dmax1 and the information that can be extracted from the QPC model.

B.-QPC model parameter extraction

See that in Figs. 1b and 2, apart from the fact that a QPC current component is detected, information related to the model parameters can be extracted. We have designed a fitting procedure where the Euclidean distance of the experimental and QPC current second derivative curves in the interval [V2dmax1-0.2V, V2dmax1+0.2V] (when it is possible) is minimized along

with the Euclidean distance of the experimental and QPC currents in the interval [0, V2dmax1]. For the two cycles represented in Fig. 1, the fitting is shown in solid lines in Fig 1b.

The fitting process was reproduced for each curve in a complete RS series with more than 2800 cycles. The QPC model parameters were obtained or calculated accordingly to a Genetic Algorithm (GA) [35]. We employed a GA for this purpose because we are dealing with a non-polynomial optimization problem and because of the appropriateness of this approach for fitting constants searching problems like ours. In our particular case, the best possible fit is selected for obtaining the QPC model parameters for each reset cycle in complex spaces, achieving good results in a reasonable run time [36]. The GA was implemented using a real-valued encoding [35], that is, each chromosome was coded as an array of 4 floating point values, each one representing a QPC parameter. We chose a stochastic uniform selection operator, along with crossover and mutation operators using constraint dependence (that is, avoiding the creation of an invalid offstpring). The crossover operator specifies how the genetic algorithm combines two individuals, or parents, to form a crossover child for the next generation. The constraint dependent crossover operator creates children that are the weighted arithmetic mean of two parents. Mutation operators specify how the genetic algorithm makes small random changes in the individuals in the population to create mutation offsprings, generally adding or subtracting a small value. Mutation provides genetic diversity and enables the genetic algorithm to search a broader space. The constraint dependent mutation operator chooses a direction (this direction will correspond to an addition or substraction) and step length that satisfies bounds and linear constraints. The

constraints are upper and lower values for each parameter (i.e., β between 0 and 1, ∝ between 0.1 eV^{-1} and 15 eV^{-1}, N between 1 and 100 and Φ between 0.25 eV and 3 eV). In (1), Φ can also be negative leading to nonlinear quantization. There is no limitation to the lower value of Φ; in this respect, if it is too negative (top of the barrier below the equilibrium Fermi level) it does not play any role. A population size of 500 chromosomes and 400 maximum generations were employed. The results are plotted in Figs. 6 and 7.

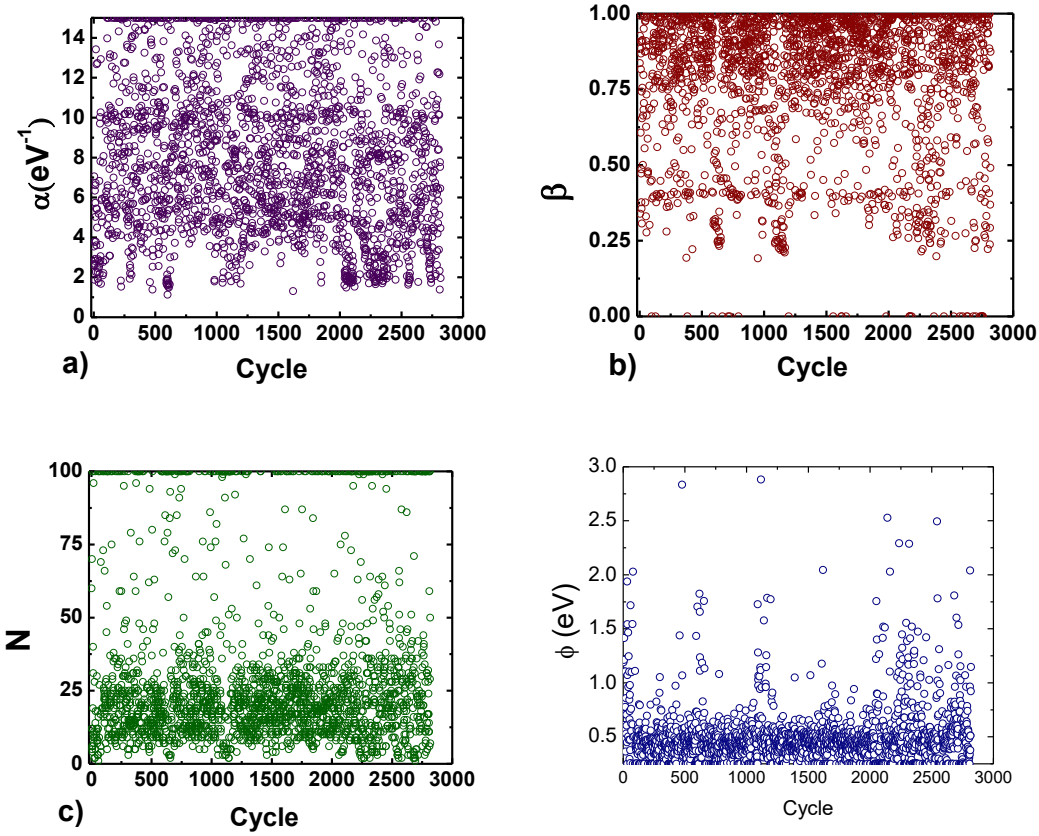

Figure 6: QPC model parameters versus cycle number for the devices under study. The calculation was performed by means of a genetic algorithm [35, 36].

See that the N parameter (number of channels) is below 25 for most cycles, Here we assume that the channels are identical, this implies similar barrier height and shape, as well as the rest of features characterized by the QPC model parameters. In addition, the barrier height (measured from the Fermi

level) is low, around 0.5 eV in most cycles. The parameters ∝ and β are more spread out in a reasonable range of values [22].

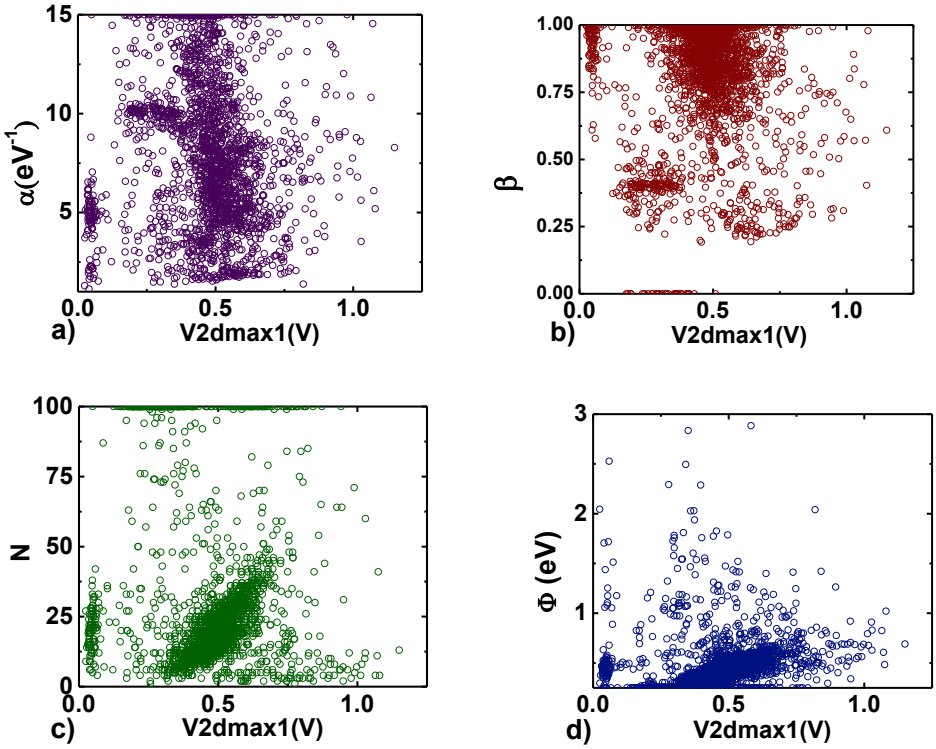

Figure 7: QPC model parameters versus V2dmax1 for the devices under study. The calculation has been performed by means of a genetic algorithm described above.

If the parameters plotted in Fig. 6 are represented versus V2dmax1 (Fig. 7) we can analyze them from another perspective. A value of V2dmax1=0.5V is seen to be the most frequent and the corresponding parameters values concentrate in a narrow interval around; in particular, N=25 and Φ=0.5 eV, β=0.85 parameters are predominant values.

The barrier thickness along the CF constriction can be calculated as shown in Eq. 2 [22],

$$t_B = \frac{h\alpha}{2\pi^2}\sqrt{\frac{2\,\Phi}{m^*}} \qquad (2)$$

where m^* is the electron effective mass, and h is Planck's constant. For this particular calculation, we take an effective mass associated with HfO_2 with a value in between $0.11m_0$ [37] and $0.44m_0$ [38]. See Fig. 8b where t_B was plotted for the cycles considered here, the most frequent value is close to 1nm as can be seen.

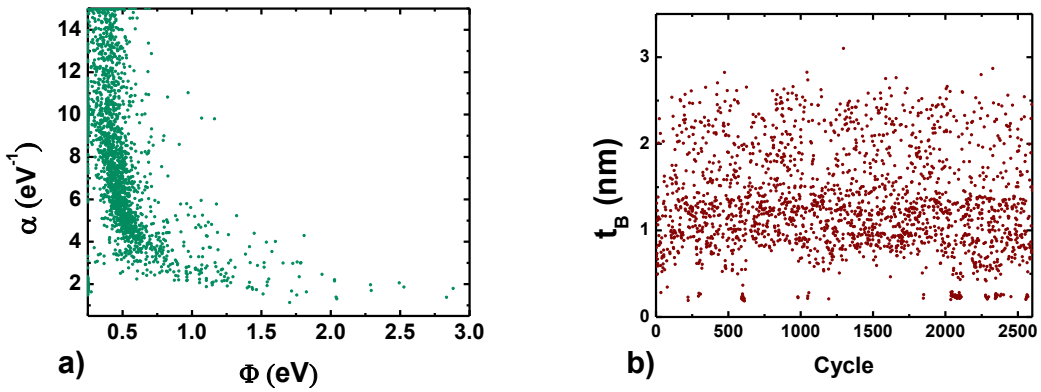

Figure 8: a) QPC model $\propto$ parameter versus Φ parameter for the RS series considered. b) Barrier thickness (calculated by means of Eq. 2) versus cycle number. The QPC parameters have been obtained by means of a genetic algorithm applied to each curve in a whole RS series.

It is worth pointing out that assuming that the device CFs are formed by Ni atoms, for $t_B \approx 1$nm there are several Ni atoms in the constriction linked to the potential barrier. There are, however, a few cases (see Fig. 8b) with $t_B \approx 0.25$nm which could correspond to a single atom constriction.

V.-CONCLUSIONS

A new screening method to detect the presence of a QPC modeled current mechanism has been developed. The new method is based on the calculation of the experimental current second derivative. The features of the second

derivative allow the detection of the QPC model fingerprints, the model parameter extraction can be performed by minimizing the Euclidean distance between the current and the current second derivative in comparison to the analytical QPC model in the context of a genetic algorithm. The extracted parameter distributions have been analyzed to characterize the device LRS low voltage quantum transport regime. Finally, a multivariate statistical analysis of the correlations between the reset voltage and other reset curve characterization parameters has been performed.

VI. - ACKNOWLEDGMENTS

UGR authors thank the support of the Spanish Ministry of Economy and Competitiveness under projects TEC2014-52152-C3-2-R and MTM2013-47929-P (also supported by the FEDER program). IMB-CNM authors thank the support of the Spanish Ministry of Economy and Competitiveness under projects TEC2014-52152-C3-1-R and TEC2014-54906-JIN (supported by the FEDER program). E. Miranda thanks the support from the ENIAC Joint Undertaking-PANACHE project. This work has made use of the Spanish ICTS Network MICRONANOFABS.

References

[1] P. Cappelletti, "Non volatile memory evolution and revolution", IEDM, p. 10.1.1-4, 2017.

[2] F. Pan, S. Gao, C. Chen, C. Song, F. Zeng, "Recent progress in resistive random access memories: materials, switching mechanisms and performance", Materials Science and Engineering, 83, pp. 1-59, 2014.

[3] D. Ielmini, R. Waser. "Resistive Switching: From Fundamentals of Nanoionic Redox Processes to Memristive Device Applications", Wiley-VCH, 2015.

[4] T. Hasegawa, K. Terabe, T. Tsuruoka, M. Aono. "Atomic Switch: Atom/Ion Movement Controlled Devices for Beyond Von-Neumann Computers", Advanced Materials, 24(2), pp. 252-267, 2012.

[5] T. Tsuruoka, K. Terabe, T. Hasegawa and M. Aono, "Forming and switching mechanisms of a cation-migration-based oxide resistive memory", Nanotechnology, *21*(42), pp. 425205, 2010.

[6] Y. C. Yang, F. Pan, Q. Liu, M. Liu, F. Zeng, "Fully room-temperature-fabricated nonvolatile resistive memory for ultrafast and high-density memory application", Nano letters, 9, pp. 1636-1643, 2009.

[7] Z. Wei, Y. Kanzawa, K. Arita, Y. Katoh, K. Kawai, S. Muraoka, S. Mitani, S. Fujii, K.Katayama, M. Iijima, T. Mikawa, T. Ninomiya, R. Miyanaga, Y. Kawashima, K. Tsuji, A. Himeno, T. Okada, R. Azuma, K. Shimakawa, H. Sugaya, T. Takagi, R. Yasuhara, K.Horiba, H. Kumigashira, M. Oshima, "Highly reliable TaOx ReRAM and direct evidence of redox reaction mechanism", IEEE International Electron Devices Meeting, pp. 1-4, 2008.

[8] S. Yu, X. Guan, H.S. Philip Wong, "On the switching parameter variation of metal oxide RRAM—Part II: Model corroboration and device design strategy", IEEE Transactions on Electron Devices, 59, pp. 1183-1188, 2012.

[9] W. Lu, D. S. Jeong , M. Kozicki , R. Waser, "Electrochemical metallization cells--blending nanoionics into nanoelectronics", MRS bulletin, 37, pp. 124, 2012.

[10] S. Gao, C. Song, C. Chen, F. Zeng, and F. Pan, "Formation process of conducting filament in planar organic resistive memory", Applied Physics Letters, 102(14), pp. 141606, 2013.

[11] R. Waser and M. Aono, "Nanoionics-based resistive switching 43

[12] M. Lanza, G. Bersuker, M. Porti, E. Miranda, M. Nafría, X. Aymerich, "Resistive switching in hafnium dioxide layers: Local phenomenon at grain boundaries", Applied Physics Letters, vol. 101, 193502, 2012.

[13] M. Lanza, "A Review on Resistive Switching in High-k Dielectrics: A Nanoscale point of View Using Conductive Atomic Force Microscope", Materials 7, pp. 2155-2182, 2014.

[14] R. Waser (ed.), "Nanoelectronics and Information Technology", 3rd ed., Wiley-VCH, Berlin, 2012.
[15] J. Zahurak, K. Miyata, M. Fischer, M. Balakrishnan, S. Chhajed,D. Wells, Li Hong, A. Torsi, J. Lim, M. Korber, K. Nakazawa, S. Mayuzumi, M. Honda, S. Sills,S. Yasuda, A. Calderoni, B. Cook, G. Damarla, H. Tran, Bei Wang, C. Cardon, K. Karda, J. Okuno, A. Johnson, T. Kunihiro, J. Sumino, M. Tsukamoto, K. Aratani, N. Ramaswamy, W. Otsuka,K. Prall. "Process integration of a 27nm, 16Gb Cu ReRAM", Electron Devices Meeting (IEDM), 2014 IEEE International, pp.6.2.1-6.2.4, 2014, doi: 10.1109/IEDM.2014.7046994
[16] T.Y. Liu, T. H. Yan, R. Scheuerlein, Y. Chen, J. K. Lee, G. Balakrishnan, G. Yee, H. Zhang, A. Yap et al., "A 130.7-mm^2 2-Layer 32-Gb ReRAM Memory Device in 24-nm Technology" IEEE J. Solid-State Circuits 49, pp. 140-153, 2014.
[17] A. Kawahara, R. Azuma, Y. Ikeda, K. Kawai, Y. Katoh, Y. Hayakawa, K. Tsuji, S. Yoneda, A. Himeno, et al., "An 8 Mb Multi-Layered Cross-Point ReRAM Macro With 443 MB/s Write Throughput", IEEE J. Solid-State Circuits 48, pp. 178-185, 2013.
[18] E. Miranda, and J. Suñé, "Modeling the conduction characteristics of broken down gate oxides in MOS structures", Microelectronics*, 40,* pp. 1599-1603, 2000.
[19] C. Acha, "Graphical analysis of current-voltage characteristics in memristive interfaces", Journal of Applied Physics, vol. 121, p. 134502, 2017.
[20] F. Jiménez-Molinos, M.A. Villena, J.B. Roldán y A.M. Roldán, "A SPICE Compact Model for Unipolar RRAM Reset Process Analysis", IEEE Transactions on Electron Devices, 62, pp. 955-962, 2015.
[21] G. González-Cordero, J.B. Roldan, F. Jiménez-Molinos, J. Suñé, S. Long y M. Liu, "A new model for bipolar RRAMs based on truncated cone conductive filaments, a Verilog-A approach", Semiconductor Science and Technology, vol 31, p. 115013, 2016.
[22] E. Miranda, and J. Suñé, "Analytic modeling of leakage current through multiple breakdown paths in SiO_2 films", *Reliability Physics Symposium, 2001. Proceedings. 39th Annual. 2001 IEEE International,* pp. 367-379, 2001.
[23] E. Miranda, C. Walczyk, C. Wenger, T. Schroeder, "Model for the Resistive Switching Effect in HfO_2 MIM Structures Based on the Transmission Properties of Narrow Constrictions", IEEE Electron Device Letters, 31, pp. 609-611, 2010.
[24] M. B. González, J. M. Rafí, O. Beldarrain, M. Zabala, and F. Campabadal, "Analysis of the switching variability in Ni/HfO2-based RRAM devices," IEEE Trans. Device Mater. Reliab., vol. 14, no. 2, pp. 769–771, 2014.
[25] M.A. Villena, M.B. González, F. Jiménez-Molinos, F. Campabadal, J.B. Roldán, J. Suñé, E. Romera, E. Miranda, "Simulation of thermal reset transitions in RRAMs including quantum effects", Journal of Applied Physics, vol. 115, pp. 214504, 2014.

[26] M.A. Villena, M.B. González, J.B. Roldán, F. Campabadal, F. Jiménez-Molinos, F.M. Gómez-Campos y J. Suñé, "An in-depth study of thermal effects in reset transitions in HfO2 based RRAMs", Solid State Electronics, 111, pp. 47-51, 2015.
[27] M.A. Villena, J.B. Roldán, M.B. González, P. González-Rodelas, F. Jiménez-Molinos, F. Campabadal, D. Barrera, "A new parameter to characterize the charge transport regime in Ni/HfO_2/Si-n^+-based RRAMs", Solid State Electronics, vol. 118, pp. 56-60, 2016.
[28] Southwick R.G., Reed J., Buu C., Butler R., Bersuker G., Knowlton W.B., "Limitations of Poole-Frenkel conduction in bilayer HfO2/SiO2 MOS devices", *IEEE Transactions on Device and materials reliability,* 10, pp. 201-207, 2010.
[29] E.W. Lim, R. Ismail, "Conduction mechanism of valence change resistive switching memory: a survey", Electronics, 4, pp. 586-613, 2015.
[30] L. M. Procel, L. Trojman, J. Moreno, F. Crupi, V. Maccaronio, R. Degraeve, L. Goux, and E. Simoen, "Experimental evidence of the quantum point contact theory in the conduction mechanism of bipolar HfO2-based resistive random access memories", Journal of Applied Physics, 114, 074509, (2013).
[31] G. Jiang and C. W. Shu, "Efficient implementation of weighted ENO schemes" Journal of Computational Physics, 126, pp. 202-228, 1996.
[32] X.D. Liu, S. Osher and T. Chan, "Weighted essentially non-oscillatory schemes", Journal of Computational Physics, 115, pp. 200-212, 1994.
[33] P. González, M.J. Ibáñez, A.M. Roldán y J.B. Roldán, "An in-depth study on WENO-based techniques to improve parameter extraction procedures in MOSFET transistors", Mathematics and Computers in Simulation, 118, pp. 248-257, 2015.
[34] D.C. Montgomery, E. A. Peck, G. G. Vining, "Introduction to linear regression analysis", Wiley, 2012.
[35] D. E. Goldberg, "Genetic Algorithms in Search, Optimization and Machine Learning", Addison-Wesley Longman Publishing Co., Inc. Boston, MA, USA, 1989.
[36] M. Kumar, M. Husian, N. Upreti and D. Gupta. "Genetic algorithm: review and application", International Journal of Information Technology and Knowledge Management, Vol. 2, pp. 451-454, 2010.
[37] S. Monaghan, P. Hurley, K. Cherkaoui, M. Negara, and A. Schenk, "Determination of electron effective mass and electron affinity in HfO2 using MOS and MOSFET structures," Solid State Electron., vol. 53, pp. 438–444, Apr. 2009.
[38] Y. Zheng, C. Troadec, A. Wee, L. Pey, S. O'Shea, and N. Chandrasekhar, "BEEM studies on metal high K-dielectric HfO2 interfaces", J. Phys.: Conf. Ser., vol. 61, pp. 1347–1351, 2007.